IET Control Theory & Applications

Brief Paper

IET Journals
The Institution of Engineering and Technology

Adaptive leader-follower formation control of non-holonomic mobile robots using active vision

ISSN 1751-8644
Received on 9th January 2014
Accepted on 24th October 2014
doi: 10.1049/iet-cta.2014.0019
www.ietdl.org

Xiaohan Chen ✉, *Yingmin Jia*

The Seventh Research Division and the Department of Systems and Control, Beihang University (BUAA), Beijing 100191, People's Republic of China
✉ *E-mail: cxhmz@163.com*

Abstract: This study is concerned with the leader-follower formation control of non-holonomic mobile robots without communication. A pan-controlled camera is the sole sensor used by the follower to observe the leader. A new vision-based formation system without range states is proposed, which eliminates the need of inter-robot range estimation. An adaptive formation controller and an adaptive camera controller are designed in the presence of unknown leader's velocities and vision-related parameters. A parameter projection algorithm is integrated into the controllers to bound the control inputs. The camera controller ensures the stable observation of the leader's features. Thus the camera constantly provides visual measurements for the formation controller which guarantees the formation maintenance. Simulation and experimental results verify the effectiveness of the proposed active vision-based formation control approach.

1 Introduction

Formation control of mobile robots has received significant attention because of its wide applications in environment exploration, search and rescue, object transportation and so on. Generally, behaviour-based [1], virtual structure-based [2, 3], graph theory-based [4] and leader-follower [5–9] approaches are applied to formation control. In particular, the leader-follower approach is welcome owing to its simplicity and scalability, although no formation feedback from the follower to the leader makes the formation structure vulnerable to disturbance [6].

Generally, robots use onboard sensors to obtain the information needed by formation controllers, especially in the absence of communication. Among all available sensors, cameras are appreciated for the rich information and low cost. Monocular vision was used in [10–13] for formation control. In [10], distributed control laws in terms of visual measurements were designed to realise parallel and circular formations, while methods to compute the visual measurements were not provided. In [11], the tool of linear quadratic regulator was used to design the platooning controller, and the relative poses between vehicles were computed by decomposing the visual homography. In [12], active contours were used for target extraction and an extended Kalman filter was employed to estimate inter-robot distances. In [13], a robust consensus protocol was proposed to estimate the global states of vision-based formation system in the scenario that each robot can only measure part of the system states.

Monocular vision could lose the observation of targets owing to its limited field of view (FOV). The use of omnidirectional vision [14–17] can avoid this problem. In [14], two methods were developed to estimate the states of vision-based formation system. The decentralised method utilised extended Kalman filters without the need of communication, while the centralised method with better state estimation required communication. In [15], a motion segmentation algorithm was proposed to compute the positions of leaders in the image plane of the follower. Input–output feedback laws were proposed in [14, 15] to realise the formation. In [16], an observability condition was derived for the omnidirectional vision-based formation system, and the inter-robot distances were estimated via an extended Kalman filter without the convergence analysis of estimation errors. As a progress, a new vision-based range estimator was designed in [17] by employing the immersion and invariance methodology, which guaranteed the global convergence of estimation errors. Input-state feedback laws were designed to stabilise the formation system in [16, 17].

Severe image distortion is the drawback limiting applications of the omnidirectional vision. As an alternative, active vision [18, 19] integrating the monocular vision with a rotational degree of freedom can overcome the FOV constraint in the monocular vision and avoid the severe image distortion in the omnidirectional vision. The active vision enables the camera to adjust its orientation towards targets. The research in [20–22] considered the active vision-based formation control. In [20, 21], inter-robot position and orientation were computed by using the special design of fiducial markers and the homography decomposition method, respectively. In [22], decentralised control laws incorporated with a single-view-based distance estimation scheme were introduced to achieve robot formation.

In this paper, we consider the active vision-based leader-follower formation control of non-holonomic mobile robots in the absence of communication. The formation configuration is shown in Fig. 1. Salient features are installed on the leader. A camera integrated with a pan platform is the only sensor equipped on the follower. Since the inter-robot communication is not established, the leader's velocities are unknown to the follower. In addition, the camera position on the follower and the feature distribution on the leader are also unknown. We propose a new vision-based leader-follower formation system without range states. A formation controller and a camera controller are designed with adaptive update laws estimating unknown parameters. The camera controller guarantees the stable observation of features. Thus, the camera can constantly provide visual measurements for the formation controller which ensures the formation maintenance.

Compared to the adaptive formation controllers designed in [3, 8], our controllers are integrated with a parameter projection algorithm [23], which confines the estimates of unknown parameters in the given bounds. Consequently, the control inputs in terms of these estimates are bounded. Such control signals are welcome in physical systems with input constraints. Notice that although the parameter projection method was also used in [7], we use a simplified version which is easier to implement in physical systems.

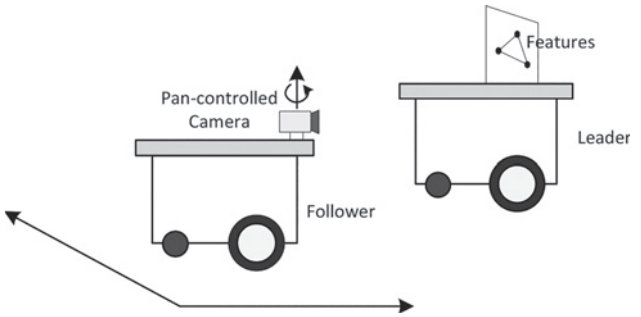

Fig. 1 *Active vision-based leader-follower setup*

The primary contribution of this paper is the introduction of a new vision-based leader-follower formation system without range states. Since the monocular vision and the omnidirectional vision cannot provide depth information, traditional formation systems containing range variables as states require the range estimation based on the visual observation [11–17, 20–22]. By contrast, our proposed formation system includes no range variables and its states can be directly computed from the visual observation. Therefore the need of range estimation is eliminated. Another contribution is that we explicitly model and control the active vision system. Although active vision was used for formation control in [20–22], the camera orientation was not explicitly controlled to observe targets.

This paper is organised as follows. In Section 2, a new vision-based leader-follower formation system is proposed, and a visual measurement scheme and an adaptive formation controller are designed. Section 3 focuses on the adaptive camera control to ensure the stable observation of visual features. Simulation and experimental results are presented in Section 4 to verify the effectiveness of our active vision-based formation control approach. Concluding remarks are given in Section 5.

2 Formation control

2.1 Vision-based leader-follower formation system

As shown in Fig. 2, two unicycle-type non-holonomic mobile robots act as the leader and the follower, respectively. Table 1 shows the definitions of variables and coordinate systems in Fig. 2. A pan-controlled camera is mounted on the follower with an offset d from the robot centre O_f to the optical centre O_c of the camera. The follower frame $O_c x_r y_r$ is fixed at O_c with y_r-axis parallel to the wheel axis. The point O_c should move to the position (X_d, Y_d) defined in the leader frame $O_l x_r y_r$ to maintain the desired formation. The formation errors X_e and Y_e are expressed in $O_c x_r y_r$. After trivial mathematical operation, we obtain the formation system [24]

$$\begin{aligned}\dot{X}_e &= -v_f + Y_e w_f + (v_l - Y_d w_l)\cos\beta - X_d w_l \sin\beta \\ \dot{Y}_e &= -(d + X_e) w_f + (v_l - Y_d w_l)\sin\beta + X_d w_l \cos\beta\end{aligned} \tag{1}$$

where v_l and w_l are linear and angular velocities of the leader, respectively, v_f and w_f are for the follower, and β is the relative orientation between the leader and the follower satisfying

$$\dot{\beta} = w_l - w_f \tag{2}$$

Since the monocular vision cannot detect the depth information, the range-related formation errors X_e and Y_e are unmeasurable. Therefore we introduce new measurable variables

$$x_e = X_e/Z_1, \quad y_e = Y_e/Z_1 \tag{3}$$

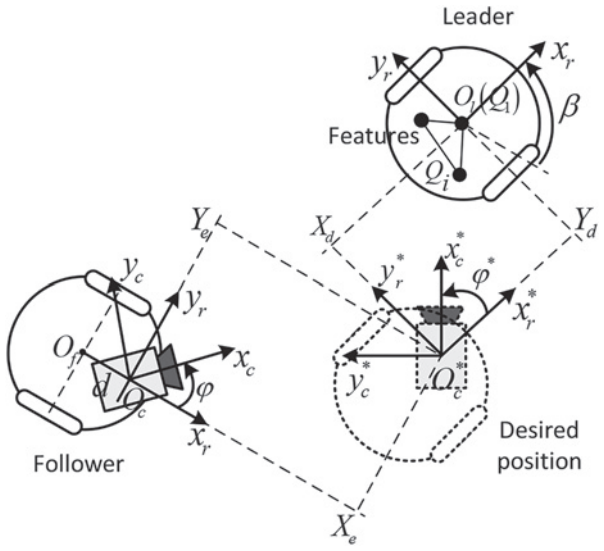

Fig. 2 *Leader-follower formation*

Table 1 Definitions of variables and coordinate systems in Fig. 2

O_l	centre of the leader
O_f	centre of the follower
O_c	optical centre of the camera
$O_l x_r y_r$	robot frame of the leader
$O_c x_r y_r$	robot frame of the follower
$O_c x_c y_c$	camera frame
(X_d, Y_d)	desired position of the follower in $O_l x_r y_r$
(X_e, Y_e)	formation errors expressed in $O_c x_r y_r$
β	relative orientation between the leader and the follower
φ	orientation of the camera with respect to the follower
d	distance between O_f and O_c

where the constant Z_1 is the height of one feature in the camera frame $O_c x_c y_c$. Then, the formation system (1) is transformed into

$$\begin{aligned}Z_1\dot{x}_e &= -v_f + Z_1 y_e w_f + v_l \cos\beta - w_z(x_d \sin\beta + y_d \cos\beta) \\ Z_1\dot{y}_e &= -d w_f - Z_1 x_e w_f + v_l \sin\beta + w_z(x_d \cos\beta - y_d \sin\beta)\end{aligned} \tag{4}$$

where

$$x_d = X_d/Z_1, \quad y_d = Y_d/Z_1, \quad w_z = w_l Z_1 \tag{5}$$

Notice that no range state is included in the formation system (4). Next, we will details the calibration of x_d and y_d, and the measurement of x_e, y_e and β.

2.2 Visual measurement

2.2.1 Camera projection model: As shown in Fig. 2, the right-hand frame $O_c x_c y_c z_c$ is fixed at the camera's optical centre with x_c-axis along the optical line and z_c-axis perpendicular to the motion plane. The feature Q_i's coordinates in $O_c x_c y_c z_c$ is denoted as (X_i, Y_i, Z_i). The perspective geometry of the camera is

$$\begin{aligned}m_i &= f_y \frac{Y_i}{X_i} + m_0 \\ n_i &= f_z \frac{Z_i}{X_i} + n_0\end{aligned} \tag{6}$$

where f_y and f_z are pixel magnification factors, (m_0, n_0) denotes the image coordinates of the camera's principal point and (m_i, n_i) is the image coordinates of Q_i. The camera's intrinsic parameters f_y, f_z, m_0 and n_0 can be obtained by the standard calibration procedure

[25]. Defining the variables

$$x_i = X_i/Z_i, \quad y_i = Y_i/Z_i \tag{7}$$

we obtain from (6) that

$$\begin{aligned} x_i &= \frac{f_z}{n_i - n_0} \\ y_i &= \frac{f_z(m_i - m_0)}{f_y(n_i - n_0)} \end{aligned} \tag{8}$$

Since m_i and n_i can be extracted from the image, (8) indicates that x_i and y_i are available from the camera observation.

2.2.2 Calibration of the desired position for the follower:

Assumption 1: At least three features are installed on the leader with the properties that:

(1) A feature (denoted as Q_1) is above the leader centre O_l (see Fig. 2).
(2) The height of each feature in the camera frame $O_c x_c y_c z_c$ is non-zero (i.e. $Z_i \neq 0$).
(3) There are three non-collinear features in a plane non-perpendicular to the motion plane of mobile robots.

Define the rotation matrix

$$R(\cdot) = \begin{bmatrix} \cos(\cdot) & -\sin(\cdot) \\ \sin(\cdot) & \cos(\cdot) \end{bmatrix} \tag{9}$$

The formation errors (X_e, Y_e), the desired follower position (X_d, Y_d) and Q_1's coordinates (X_1, Y_1) in the camera frame $O_c x_c y_c$ are related by

$$\begin{bmatrix} X_e \\ Y_e \end{bmatrix} = R(\varphi) \begin{bmatrix} X_1 \\ Y_1 \end{bmatrix} + R(\beta) \begin{bmatrix} X_d \\ Y_d \end{bmatrix} \tag{10}$$

where φ is the camera orientation with respect to the follower (see Fig. 2) and can be read from the encoder installed on the pan platform, $R(\varphi)$ is the coordinate transformation from $O_c x_c y_c$ to $O_c x_r y_r$ and $R(\beta)$ is the coordinate transformation from $O_l x_c y_c$ to $O_c x_r y_r$.

We move the follower to its desired position with the orientation parallel with the leader's orientation (i.e. $X_e = Y_e = 0$ and $\beta = 0$). The camera orientation is adjusted to keep all features observed. At this desired state, the follower frame is denoted as $O_c^* x_r^* y_r^*$, the camera frame as $O_c^* x_c^* y_c^*$, and the values of φ, X_i, Y_i, Z_i, m_i and n_i as φ^*, X_i^*, Y_i^*, Z_i^*, m_i^* and n_i^*, respectively, (see Fig. 2). Then, we have from (10) that

$$\begin{bmatrix} X_d \\ Y_d \end{bmatrix} = -R(\varphi^*) \begin{bmatrix} X_1^* \\ Y_1^* \end{bmatrix} \tag{11}$$

where $R(\varphi^*)$ is the coordinate transformation from $O_c^* x_c^* y_c^*$ to $O_c^* x_r^* y_r^*$. Notice that $Z_i \equiv Z_i^*$ because of the planar motion of the robots and the camera. According to (5), (7), (8) and (11), we obtain

$$\begin{bmatrix} x_d \\ y_d \end{bmatrix} = \begin{bmatrix} X_d/Z_1^* \\ Y_d/Z_1^* \end{bmatrix} = -R(\varphi^*) \begin{bmatrix} X_1^*/Z_1^* \\ Y_1^*/Z_1^* \end{bmatrix} = -R(\varphi^*) \begin{bmatrix} x_1^* \\ y_1^* \end{bmatrix} \tag{12}$$

where

$$\begin{aligned} x_i^* &= \frac{X_i^*}{Z_i^*} = \frac{f_z}{n_i^* - n_0} \\ y_i^* &= \frac{Y_i^*}{Z_i^*} = \frac{f_z(m_i^* - m_0)}{f_y(n_i^* - n_0)} \end{aligned} \tag{13}$$

Since m_i^*, n_i^* and φ^* are measurable, x_i^*, y_i^*, x_d and y_d are available.

2.2.3 State measurement:

As shown in Fig. 2, the geometric analysis gives

$$\begin{bmatrix} X_i \\ Y_i \end{bmatrix} = R(-\varphi + \varphi^* + \beta) \begin{bmatrix} X_i^* \\ Y_i^* \end{bmatrix} + R(-\varphi) \begin{bmatrix} X_e \\ Y_e \end{bmatrix} \tag{14}$$

where $R(-\varphi + \varphi^* + \beta)$ is the coordinate transformation from $O_c^* x_c^* y_c^*$ to $O_c x_c y_c$, and $R(-\varphi)$ is the coordinate transformation from $O_c x_r y_r$ to $O_c x_c y_c$. Consequently, we have from (14) that

$$\begin{bmatrix} X_e/Z_i \\ Y_e/Z_i \end{bmatrix} = R(\varphi) \begin{bmatrix} X_i/Z_i \\ Y_i/Z_i \end{bmatrix} - R(\varphi^* + \beta) \begin{bmatrix} X_i^*/Z_i^* \\ Y_i^*/Z_i^* \end{bmatrix} \tag{15}$$

In view of (7) and (13), the above equation is rewritten as

$$\begin{aligned} X_e/Z_i &= x_i \cos\varphi - y_i \sin\varphi - x_i^* \cos(\varphi^* + \beta) + y_i^* \sin(\varphi^* + \beta) \\ Y_e/Z_i &= x_i \sin\varphi + y_i \cos\varphi - x_i^* \sin(\varphi^* + \beta) - y_i^* \cos(\varphi^* + \beta) \end{aligned} \tag{16}$$

Since for the features Q_i and Q_j

$$(X_e/Z_i)(Y_e/Z_j) - (Y_e/Z_i)(X_e/Z_j) = 0 \tag{17}$$

we obtain from (16) that

$$a_{ij} \sin\Delta + b_{ij} \cos\Delta = c_{ij} \tag{18}$$

where

$$\begin{aligned} \Delta &= -\varphi + \varphi^* + \beta \\ a_{ij} &= -x_i x_j^* - y_i y_j^* + y_i^* y_j + x_i^* x_j \\ b_{ij} &= -x_i y_j^* + y_i x_j^* - x_i^* y_j + y_i^* x_j \\ c_{ij} &= -x_i y_j + y_i x_j - x_i^* y_j^* + y_i^* x_j^* \end{aligned} \tag{19}$$

If there are N $(N \geq 3)$ features observed by the camera, it can be obtained that

$$\begin{bmatrix} \sin\Delta \\ \cos\Delta \end{bmatrix} = (C^T C)^{-1} C^T D \tag{20}$$

where

$$C = \begin{bmatrix} a_{12} & b_{12} \\ a_{13} & b_{13} \\ \vdots & \vdots \\ a_{N-1,N} & b_{N-1,N} \end{bmatrix}, \quad D = \begin{bmatrix} c_{12} \\ c_{13} \\ \vdots \\ c_{N-1,N} \end{bmatrix} \tag{21}$$

Assume that the solved values are $\sin\Delta = s_\Delta$ and $\cos\Delta = c_\Delta$. The optimal estimate of β is

$$\beta = \text{atan2}(s_\Delta, c_\Delta) + \varphi - \varphi^* \tag{22}$$

Furthermore, we obtain from (3), (5), (7) and (10) that

$$\begin{bmatrix} x_e \\ y_e \end{bmatrix} = R(\beta) \begin{bmatrix} x_d \\ y_d \end{bmatrix} + R(\varphi) \begin{bmatrix} x_1 \\ y_1 \end{bmatrix} \tag{23}$$

which indicates x_e and y_e are available.

Remark 1: Assumption 1 consists of the requirements on the feature distribution. We do not need the information of the relative positions between features. The last property in Assumption 1 ensures that the rank of $C^T C$ is two (see appendix in [26]), and more features yield a better estimate of β.

2.3 Formation controller design

In (4), the offset d and the height Z_1 are unknown since the camera's optical centre O_c is inaccessible. The leader's velocities v_l and w_l are unknown to the follower because of no inter-robot communication. Without loss of generality, Z_1 is assumed to be positive. Further, we assume that the bounds of v_l, w_l, $\dot{v}_l$, $\dot{w}_l$, d and Z_1 are known.

IET Control Theory Appl., 2015, Vol. 9, Iss. 8, pp. 1302–1311

Assumption 2: There are known positive constants σ, $\underline{c}_{\rm d}$, $\bar{c}_{\rm d}$, $\underline{c}_z$, $\bar{c}_z$, $\underline{c}_v$, $\bar{c}_v$, $\bar{c}_w$, $\bar{a}_v$ and $\bar{a}_w$ so that

$$\begin{aligned}&\underline{c}_{\rm d}+\sigma<d<\bar{c}_{\rm d}-\sigma\\&\underline{c}_z+\sigma<Z_{\rm l}<\bar{c}_z-\sigma\\&\underline{c}_v+\sigma<v_{\rm l}<\bar{c}_v-\sigma\\&|w_{\rm l}|<\bar{c}_w-\sigma,\quad |\dot{v}_{\rm l}|<\bar{a}_v,\quad |\dot{w}_{\rm l}|<\bar{a}_w\end{aligned}\tag{24}$$

Remark 2: In view of (5) and (24), we can find suitable constants $\underline{\lambda}_w$ and $\bar{\lambda}_w$ such that

$$\underline{\lambda}_w+\sigma<w_z<\bar{\lambda}_w-\sigma\tag{25}$$

Design the formation controller

$$\begin{aligned}v_{\rm f}&=\hat{v}_{\rm l}\cos\beta-\hat{w}_z(x_{\rm d}\sin\beta+y_{\rm d}\cos\beta)+k_x x_{\rm e}\\w_{\rm f}&=[\hat{v}_{\rm l}\sin\beta+\hat{w}_z(x_{\rm d}\cos\beta-y_{\rm d}\sin\beta)+k_y y_{\rm e}]/\hat{d}\end{aligned}\tag{26}$$

where k_x and k_y are positive feedback gains and $\hat{d}$, $\hat{v}_{\rm l}$ and $\hat{w}_z$ are the estimates of d, $v_{\rm l}$ and w_z, respectively.

Define the Lyapunov function

$$V=\frac{1}{2}\left(Z_{\rm l}(x_{\rm e}^2+y_{\rm e}^2)+\frac{1}{\gamma_{\rm d}}\tilde{d}^2+\frac{1}{\gamma_v}\tilde{v}_{\rm l}^2+\frac{1}{\gamma_w}\tilde{w}_z^2\right)\tag{27}$$

where $\tilde{d}=d-\hat{d}$, $\tilde{v}_{\rm l}=v_{\rm l}-\hat{v}_{\rm l}$, $\tilde{w}_z=w_z-\hat{w}_z$ and $\gamma_{\rm d}$, γ_v, γ_w are positive constants. With the controller (26), the time derivative of V along the solution of (4) is

$$\begin{aligned}\dot{V}=&-k_x x_{\rm e}^2-k_y y_{\rm e}^2-\frac{\tilde{d}}{\gamma_{\rm d}}(\dot{\tilde{d}}-\gamma_{\rm d}\Omega_{\rm d})-\frac{\tilde{v}_{\rm l}}{\gamma_v}(\dot{\hat{v}}_{\rm l}-\gamma_v\Omega_v)\\&-\frac{\tilde{w}_z}{\gamma_w}(\dot{\hat{w}}_z-\gamma_w\Omega_w)+\frac{\tilde{v}_{\rm l}}{\gamma_v}\dot{v}_{\rm l}+\frac{\tilde{w}_z}{\gamma_w}\dot{w}_z\end{aligned}\tag{28}$$

where

$$\begin{aligned}\Omega_{\rm d}&=-w_{\rm f}y_{\rm e}\\\Omega_v&=x_{\rm e}\cos\beta+y_{\rm e}\sin\beta\\\Omega_w&=-x_{\rm e}(x_{\rm d}\sin\beta+y_{\rm d}\cos\beta)+y_{\rm e}(x_{\rm d}\cos\beta-y_{\rm d}\sin\beta)\end{aligned}\tag{29}$$

The parameter projection algorithm [23] is used to design the update laws

$$\dot{\hat{d}}=\begin{cases}\gamma_{\rm d}\Omega_{\rm d} & \underline{c}_{\rm d}+\sigma<\hat{d}<\bar{c}_{\rm d}-\sigma\\\gamma_{\rm d}\Omega_{\rm d}+|\gamma_{\rm d}\Omega_{\rm d}|+\varepsilon_{\rm d} & \hat{d}\le\underline{c}_{\rm d}+\sigma\\\gamma_{\rm d}\Omega_{\rm d}-|\gamma_{\rm d}\Omega_{\rm d}|-\varepsilon_{\rm d} & \hat{d}\ge\bar{c}_{\rm d}-\sigma\end{cases}\tag{30}$$

$$\dot{\hat{v}}_{\rm l}=\begin{cases}\gamma_v\Omega_v & \underline{c}_v+\sigma<\hat{v}_{\rm l}<\bar{c}_v-\sigma\\\gamma_v\Omega_v+|\gamma_v\Omega_v|+\varepsilon_v & \hat{v}_{\rm l}\le\underline{c}_v+\sigma\\\gamma_v\Omega_v-|\gamma_v\Omega_v|-\varepsilon_v & \hat{v}_{\rm l}\ge\bar{c}_v-\sigma\end{cases}\tag{31}$$

$$\dot{\hat{w}}_z=\begin{cases}\gamma_w\Omega_w & \underline{\lambda}_w+\sigma<\hat{w}_z<\bar{\lambda}_w-\sigma\\\gamma_w\Omega_w+|\gamma_w\Omega_w|+\varepsilon_w & \hat{w}_z\le\underline{\lambda}_w+\sigma\\\gamma_w\Omega_w-|\gamma_w\Omega_w|-\varepsilon_w & \hat{w}_z\ge\bar{\lambda}_w-\sigma\end{cases}\tag{32}$$

where $\varepsilon_{\rm d}$, ε_v and ε_w are small positive constants.

Theorem 1: Consider the formation system (4) under Assumption 2. If the controller (26) with the update laws (30)–(32) is applied, then the formation errors $x_{\rm e}$ and $y_{\rm e}$ can be arbitrarily small by tuning k_x, k_y, $\gamma_{\rm d}$, γ_v and γ_w.

Proof: It is observed from (24) and (30) that $\tilde{d}(\dot{\tilde{d}}-\gamma_{\rm d}\Omega_{\rm d})=-\tilde{d}(|\gamma_{\rm d}\Omega_{\rm d}|+\varepsilon_{\rm d})>0$ when $\hat{d}\ge\bar{c}_{\rm d}-\sigma>d$, $\tilde{d}(\dot{\tilde{d}}-\gamma_{\rm d}\Omega_{\rm d})=\tilde{d}(|\gamma_{\rm d}\Omega_{\rm d}|+\varepsilon_{\rm d})>0$ when $\hat{d}\le\underline{c}_{\rm d}+\sigma<d$, and $\tilde{d}(\dot{\tilde{d}}-\gamma_{\rm d}\Omega_{\rm d})=0$ when $\underline{c}_{\rm d}+\sigma<\hat{d}<\bar{c}_{\rm d}-\sigma$. Therefore $\tilde{d}(\dot{\tilde{d}}-\gamma_{\rm d}\Omega_{\rm d})\ge 0$ holds for $\hat{d}$ updated as (30). Similarly, we obtain $\tilde{v}_{\rm l}(\dot{\hat{v}}_{\rm l}-\gamma_v\Omega_v)\ge 0$ and $\tilde{w}_z(\dot{\hat{w}}_z-\gamma_w\Omega_w)\ge 0$ for $\hat{v}_{\rm l}$ and $\hat{w}_z$ updated as (31) and (32). Substituting (30)–(32) into (28), we have

$$\begin{aligned}\dot{V}&\le-k_x x_{\rm e}^2-k_y y_{\rm e}^2+\frac{\tilde{v}_{\rm l}}{\gamma_v}\dot{v}_{\rm l}+\frac{\tilde{w}_z}{\gamma_w}\dot{w}_z\\&\le-\frac{2\underline{k}}{Z_{\rm l}}V+\frac{\underline{k}}{Z_{\rm l}\gamma_{\rm d}}\tilde{d}^2+\frac{\underline{k}}{Z_{\rm l}\gamma_v}\tilde{v}_{\rm l}^2+\frac{\underline{k}}{Z_{\rm l}\gamma_w}\tilde{w}_z^2+\frac{1}{\gamma_v}\tilde{v}_{\rm l}\dot{v}_{\rm l}+\frac{1}{\gamma_w}\tilde{w}_z\dot{w}_z\\&\le-\frac{2\underline{k}}{Z_{\rm l}}V+E\end{aligned}\tag{33}$$

where $\underline{k}=\min\{k_x,k_y\}$ and

$$\begin{aligned}E=&\frac{\underline{k}}{Z_{\rm l}\gamma_{\rm d}}(\bar{c}_{\rm d}-\underline{c}_{\rm d})^2+\frac{\underline{k}}{Z_{\rm l}\gamma_v}(\bar{c}_v-\underline{c}_v)^2+\frac{\underline{k}}{Z_{\rm l}\gamma_w}(\bar{\lambda}_w-\underline{\lambda}_w)^2\\&+\frac{1}{\gamma_v}(\bar{c}_v-\underline{c}_v)\bar{a}_v+\frac{1}{\gamma_w}(\bar{\lambda}_w-\underline{\lambda}_w)\bar{a}_w\bar{c}_z\end{aligned}\tag{34}$$

It is obtained by using the comparison principle [27] that

$$V(t)\le\left(V(0)-\frac{Z_{\rm l}E}{2\underline{k}}\right)e^{-2\underline{k}t/Z_{\rm l}}+\frac{Z_{\rm l}E}{2\underline{k}}\tag{35}$$

The last term in (35) can be small enough by increasing k_x, k_y, $\gamma_{\rm d}$, γ_v and γ_w. Therefore V can be ultimately bounded in an arbitrarily small neighbourhood of zero, which means that the formation errors $x_{\rm e}$ and $y_{\rm e}$ can be arbitrarily small. □

Remark 3: Theorem 1 shows that $E/\underline{k}$ decreases as the control parameters k_x, k_y, $\gamma_{\rm d}$, γ_v and γ_w increase, and consequently the formation errors $x_{\rm e}$ and $y_{\rm e}$ will converge fast to a small neighbourhood of zero. However, the increments of k_x and k_y lead to large control inputs [see (26)]. Besides, increasing $\gamma_{\rm d}$, γ_v and γ_w accelerates the update rates of $\hat{d}$, $\hat{v}_{\rm l}$ and $\hat{w}_z$ [see (30)–(32)]. Then the controller (26) is more sensitive to disturbances, which yields the chattering of control inputs in practical systems. Thus, the control parameters k_x, k_y, $\gamma_{\rm d}$, γ_v and γ_w should be adjusted to be small when the residual formation errors are acceptable.

Remark 4: The initial estimates of d, $v_{\rm l}$ and w_z are set in their given bounds (i.e. $\underline{c}_{\rm d}\le\hat{d}(0)\le\bar{c}_{\rm d}$, $\underline{c}_v\le\hat{v}_{\rm l}(0)\le\bar{c}_v$ and $\underline{\lambda}_w\le\hat{w}_z(0)\le\bar{\lambda}_w$). Since $\dot{\hat{d}}\le-\varepsilon_{\rm d}<0$ for $\hat{d}\ge\bar{c}_{\rm d}-\sigma$ and $\dot{\hat{d}}\ge\varepsilon_{\rm d}>0$ for $\hat{d}\le\underline{c}_{\rm d}+\sigma$ [see (30)], $\underline{c}_{\rm d}\le\hat{d}\le\bar{c}_{\rm d}$ always holds for $\underline{c}_{\rm d}\le\hat{d}(0)\le\bar{c}_{\rm d}$. Similarly, $\underline{c}_v\le\hat{v}_{\rm l}\le\bar{c}_v$ for $\underline{c}_v\le\hat{v}_{\rm l}(0)\le\bar{c}_v$ and $\underline{\lambda}_w\le\hat{w}_z\le\bar{\lambda}_w$ for $\underline{\lambda}_w\le\hat{w}_z(0)\le\bar{\lambda}_w$. In other words, the update laws (30)–(32) guarantee that $\hat{d}$, $\hat{v}_{\rm l}$ and $\hat{w}_z$ are constrained in the given bounds. Consequently, the control inputs generated by (26) are bounded. In view of (24), (27) and (35), we have

$$x_{\rm e}^2,y_{\rm e}^2\le\frac{2V}{Z_{\rm l}}\le\max\left\{\frac{2V(0)}{\underline{c}_z},\frac{E}{\underline{k}}\right\}=F\tag{36}$$

Then according to (24) and (26), we obtain

$$\begin{aligned}|v_{\rm f}|&\le\bar{c}_v+\bar{\lambda}_w\sqrt{x_{\rm d}^2+y_{\rm d}^2}+k_x\sqrt{F}\\|w_{\rm f}|&\le(\bar{c}_v+\bar{\lambda}_w\sqrt{x_{\rm d}^2+y_{\rm d}^2}+k_y\sqrt{F})/\underline{c}_{\rm d}\end{aligned}\tag{37}$$

Remark 5: According to (2) and (26), the internal dynamics of the formation system (4) is

$$\dot{\beta} = -\frac{\hat{v}_1}{\hat{d}}\sin\beta + w_1 - \frac{\hat{w}_z}{\hat{d}}(x_d\cos\beta - y_d\sin\beta) - \frac{k_y}{\hat{d}}y_e \tag{38}$$

Since y_e is ultimately bounded, it is obtained from (24), (30) and (32) that there exists a constant τ so that

$$\left|w_1 - \frac{\hat{w}_z}{\hat{d}}(x_d\cos\beta - y_d\sin\beta) - \frac{k_y}{\hat{d}}y_e\right| \le \tau \tag{39}$$

Recall that $\hat{v}_1 \ge \underline{c}_v > 0$ and $0 < \underline{c}_d \le \hat{d} \le \bar{c}_d$. Similar to the analysis in [24], β is bounded if $\underline{c}_v/\bar{c}_d > \tau$.

Corollary 1: Consider the formation system (4) under Assumption 2. If the leader moves with constant linear and angular velocities and the controller (26) with the update laws (30)–(32) is applied to the follower, then the formation errors x_e and y_e will converge to zero.

Proof: If v_1 and w_1 are constant, then $\dot{v}_1 = 0$ and $\dot{w}_z = Z_1\dot{w}_1 = 0$. According to (33), we have

$$\dot{V} \le -k_x x_e^2 - k_y y_e^2 \tag{40}$$

It is obtained that V is non-increasing and x_e, y_e are bounded. According to (4), (24) and (37), $\dot{x}_e$ and $\dot{y}_e$ are bounded. Thus, x_e^2 and y_e^2 are uniformly continuous. Applying Barbalat's lemma [27] ensures that x_e and y_e converge to zero, since

$$\int_0^\infty k_x x_e^2 dt + \int_0^\infty k_y y_e^2\, dt \le \int_0^\infty -\dot{V} dt = V(0) - V(\infty) \le V(0) \tag{41}$$

□

3 Camera control

3.1 Pan-controlled camera

In order to keep all features observed, the feature Q_1, which is regarded as the reference point, is expected to stay around the image centre. Differentiating both sides of (10) and using (1) and (2), we obtain

$$\begin{bmatrix}\dot{X}_1\\ \dot{Y}_1\end{bmatrix} = \begin{bmatrix}(w_c + w_f)Y_1 - v_f\cos\varphi - dw_f\sin\varphi + v_1\cos(\beta-\varphi)\\ -(w_c + w_f)X_1 + v_f\sin\varphi - dw_f\cos\varphi + v_1\sin(\beta-\varphi)\end{bmatrix} \tag{42}$$

where $w_c = \dot{\varphi}$ is the angular velocity of the camera with respect to the follower.

In view of (6), define the image errors

$$\begin{aligned} e_y &= m_1 - m_0 = f_y\frac{Y_1}{X_1}\\ e_z &= n_1 - n_0 = f_z\frac{Z_1}{X_1}\end{aligned} \tag{43}$$

Their derivatives are

$$\begin{aligned} \dot{e}_y &= f_y\frac{\dot{Y}_1}{X_1} - e_y\frac{\dot{X}_1}{X_1}\\ \dot{e}_z &= -e_z\frac{\dot{X}_1}{X_1}\end{aligned} \tag{44}$$

Substituting (42) and (43) into (44) yields

$$\begin{aligned} \dot{e}_y = &-\left(f_y + \frac{e_y^2}{f_y}\right)(w_c + w_f)\\ &+ \frac{d}{Z_1}\frac{e_z}{f_z}w_f(-f_y\cos\varphi + e_y\sin\varphi)\\ &+ \frac{1}{Z_1}\frac{e_z}{f_z}v_f(f_y\sin\varphi + e_y\cos\varphi)\\ &+ \frac{v_1}{Z_1}\frac{e_z}{f_z}(f_y\sin(\beta-\varphi) - e_y\cos(\beta-\varphi))\\ \dot{e}_z = &-\frac{e_y e_z}{f_y}(w_c + w_f) + \frac{d}{Z_1}\frac{e_z^2}{f_z}w_f\sin\varphi\\ &+ \frac{1}{Z_1}\frac{e_z^2}{f_z}v_f\cos\varphi - \frac{v_1}{Z_1}\frac{e_z^2}{f_z}\cos(\beta-\varphi)\end{aligned} \tag{45}$$

Rewrite the first equation of (45) as

$$\dot{e}_y = -\left(f_y + \frac{e_y^2}{f_y}\right)(w_c + w_f) + d_z\Phi_d + \alpha\Phi_\alpha + v_z\Phi_v \tag{46}$$

where $d_z = d/Z_1$, $\alpha = 1/Z_1$, $v_z = v_1/Z_1$ and

$$\begin{aligned} \Phi_d &= \frac{e_z}{f_z}w_f(-f_y\cos\varphi + e_y\sin\varphi)\\ \Phi_\alpha &= \frac{e_z}{f_z}v_f(f_y\sin\varphi + e_y\cos\varphi)\\ \Phi_v &= \frac{e_z}{f_z}(f_y\sin(\beta-\varphi) - e_y\cos(\beta-\varphi))\end{aligned} \tag{47}$$

3.2 Camera controller design

According to (24), we can find positive constants $\underline{\lambda}_d$, $\bar{\lambda}_d$, $\underline{\lambda}_\alpha$, $\bar{\lambda}_\alpha$, $\underline{\lambda}_v$, $\bar{\lambda}_v$ and δ so that

$$\begin{aligned} \underline{\lambda}_d + \delta < d_z < \bar{\lambda}_d - \delta\\ \underline{\lambda}_\alpha + \delta < \alpha < \bar{\lambda}_\alpha - \delta\\ \underline{\lambda}_v + \delta < v_z < \bar{\lambda}_v - \delta\end{aligned} \tag{48}$$

Design the camera controller

$$w_c = -w_f + \frac{1}{f_y + e_y^2/f_y}\left(\hat{d}_z\Phi_d + \hat{\alpha}\Phi_\alpha + \hat{v}_z\Phi_v + k_c e_y\right) \tag{49}$$

where k_c is a positive feedback gain and $\hat{d}_z$, $\hat{\alpha}$, $\hat{v}_z$ are the estimates of d_z, α, v_z, respectively. The estimation errors are $\tilde{d}_z = d_z - \hat{d}_z$, $\tilde{\alpha} = \alpha - \hat{\alpha}$ and $\tilde{v}_z = v_z - \hat{v}_z$.

Choose the Lyapunov function

$$V_c = \frac{1}{2}\left(e_y^2 + \frac{1}{\mu_d}\tilde{d}_z^2 + \frac{1}{\mu_\alpha}\tilde{\alpha}^2 + \frac{1}{\mu_v}\tilde{v}_z^2\right) \tag{50}$$

where μ_d, μ_α and μ_v are positive constants. Substituting (46) and (49) into the derivative of V_c gives

$$\begin{aligned} \dot{V}_c = &-k_c e_y^2 - \frac{\tilde{d}_z}{\mu_d}(\dot{\hat{d}}_z - \mu_d e_y\Phi_d) - \frac{\tilde{\alpha}}{\mu_\alpha}(\dot{\hat{\alpha}} - \mu_\alpha e_y\Phi_\alpha)\\ &- \frac{\tilde{v}_z}{\mu_v}(\dot{\hat{v}}_z - \mu_v e_y\Phi_v) + \frac{\tilde{v}_z}{\mu_v}\dot{v}_z\end{aligned} \tag{51}$$

Design the update laws

$$\dot{\hat{d}}_z = \begin{cases} \mu_d e_y \Phi_{\mathrm{d}} & \underline{\lambda}_{\mathrm{d}} + \delta < \hat{d}_z < \bar{\lambda}_{\mathrm{d}} - \delta \\ \mu_{\mathrm{d}} e_y \Phi_{\mathrm{d}} + |\mu_{\mathrm{d}} e_y \Phi_{\mathrm{d}}| + \eta_{\mathrm{d}} & \hat{d}_z \le \underline{\lambda}_{\mathrm{d}} + \delta \\ \mu_{\mathrm{d}} e_y \Phi_{\mathrm{d}} - |\mu_{\mathrm{d}} e_y \Phi_{\mathrm{d}}| - \eta_{\mathrm{d}} & \hat{d}_z \ge \bar{\lambda}_{\mathrm{d}} - \delta \end{cases} \tag{52}$$

$$\dot{\hat{\alpha}} = \begin{cases} \mu_\alpha e_y \Phi_\alpha & \underline{\lambda}_\alpha + \delta < \hat{\alpha} < \bar{\lambda}_\alpha - \delta \\ \mu_\alpha e_y \Phi_\alpha + |\mu_\alpha e_y \Phi_\alpha| + \eta_\alpha & \hat{\alpha} \le \underline{\lambda}_\alpha + \delta \\ \mu_\alpha e_y \Phi_\alpha - |\mu_\alpha e_y \Phi_\alpha| - \eta_\alpha & \hat{\alpha} \ge \bar{\lambda}_\alpha - \delta \end{cases} \tag{53}$$

$$\dot{\hat{v}}_z = \begin{cases} \mu_v e_y \Phi_v & \underline{\lambda}_v + \delta < \hat{v}_z < \bar{\lambda}_v - \delta \\ \mu_v e_y \Phi_v + |\mu_v e_y \Phi_v| + \eta_v & \hat{v}_z \le \underline{\lambda}_v + \delta \\ \mu_v e_y \Phi_v - |\mu_v e_y \Phi_v| - \eta_v & \hat{v}_z \ge \bar{\lambda}_v - \delta \end{cases} \tag{54}$$

where η_{d}, η_α and η_v are small positive constants.

Theorem 2: Apply the camera controller (49) with the update laws (52)–(54) to the system (45). Then the image error e_y can arbitrarily approach zero by tuning k_{c}, μ_{d}, μ_α and μ_v.

Proof: Similar to the proof of Theorem 1, we have $\tilde{d}_z(\dot{\hat{d}}_z - \mu_{\mathrm{d}} e_y \Phi_{\mathrm{d}}) \ge 0$, $\tilde{\alpha}(\dot{\hat{\alpha}} - \mu_\alpha e_y \Phi_\alpha) \ge 0$ and $\tilde{v}_z(\dot{\hat{v}}_z - \mu_v e_y \Phi_v) \ge 0$ for $\hat{d}_z$, $\hat{\alpha}$ and $\hat{v}_z$ updated as (52)–(54). Then, we obtain from (51) that

$$\begin{aligned} \dot{V}_{\mathrm{c}} &\le -k_{\mathrm{c}} e_y^2 + \frac{\tilde{v}_z}{\mu_v}\dot{v}_z \\ &\le -2k_{\mathrm{c}} V_{\mathrm{c}} + \frac{k_{\mathrm{c}}}{\mu_{\mathrm{d}}}\tilde{d}_z^2 + \frac{k_{\mathrm{c}}}{\mu_\alpha}\tilde{\alpha}^2 + \frac{k_{\mathrm{c}}}{\mu_v}\tilde{v}_z^2 + \frac{\tilde{v}_z}{\mu_v}\dot{v}_z \\ &\le -2k_{\mathrm{c}} V_{\mathrm{c}} + G \end{aligned} \tag{55}$$

with

$$\begin{aligned} G = &\frac{k_{\mathrm{c}}}{\mu_{\mathrm{d}}}(\bar{\lambda}_{\mathrm{d}} - \underline{\lambda}_{\mathrm{d}})^2 + \frac{k_{\mathrm{c}}}{\mu_\alpha}(\bar{\lambda}_\alpha - \underline{\lambda}_\alpha)^2 \\ &+ \frac{k_{\mathrm{c}}}{\mu_v}(\bar{\lambda}_v - \underline{\lambda}_v)^2 + \frac{\bar{a}_v}{\mu_v \underline{c}_z}(\bar{\lambda}_v - \underline{\lambda}_v) \end{aligned} \tag{56}$$

Using the comparison principle [27], we have

$$V_{\mathrm{c}}(t) \le \left(V_{\mathrm{c}}(0) - \frac{G}{2k_{\mathrm{c}}}\right) e^{-2k_{\mathrm{c}}t} + \frac{G}{2k_{\mathrm{c}}} \tag{57}$$

Since increasing k_{c}, μ_{d}, μ_α and μ_v can make G/k_{c} small enough, V_{c} can arbitrarily approach zero. It means that the image error e_y can be arbitrarily small. □

Remark 6: Theorem 2 shows that G/k_{c} decreases with the increments of k_{c}, μ_{d}, μ_α and μ_v, and then the image error e_y will converge fast to a small neighbourhood of zero. However, large k_{c} leads to large control input for the pan platform [see (49)], and the increase of μ_{d}, μ_α and μ_v accelerates the update rates of $\hat{d}_z$, $\hat{\alpha}$ and $\hat{v}_z$. Then, the camera controller (49) is more sensitive to disturbances, which leads to the chattering of control input. Therefore the control parameters k_{c}, μ_{d}, μ_α and μ_v should be set small when the residual image error e_y is acceptable.

Remark 7: The initial estimates of d_z, α and v_z are set in their given bounds (i.e. $\underline{\lambda}_{\mathrm{d}} \le \hat{d}_z(0) \le \bar{\lambda}_{\mathrm{d}}$, $\underline{\lambda}_\alpha \le \hat{\alpha}(0) \le \bar{\lambda}_\alpha$ and $\underline{\lambda}_v \le \hat{v}_z(0) \le \bar{\lambda}_v$). Similar to the analysis in Remark 4, the update laws (52)–(54) ensure that $\hat{d}_z$, $\hat{\alpha}$ and $\hat{v}_z$ are constrained in the given bounds. Consequently, w_{c} is bounded.

Remark 8: The image error e_z is not directly controlled. In view of (43), e_z is inversely proportional to X_1. Since the camera is controlled by (49) to face to the feature Q_1, the magnitude of X_1 approximates to the distance between the leader and the camera. Assume that all features are observed by the camera at proper positions in the image plane when the follower is at the desired position. Then the features will not leave the camera's FOV along the z_{c}-axis when the follower approaches its desired position forward.

4 Simulation and experimental results

4.1 Simulation results

As shown in Fig. 3, four mobile robots are expected to realise a diamond formation. Robot 1 acts as the leader for Robots 2 and 4. Robot 2 is the leader of Robot 3. The desired positions of Robots 2 and 4 in the local frame of Robot 1 are $(-1\,\mathrm{m}, -0.5\,\mathrm{m})$ and $(-1\,\mathrm{m}, 0.5\,\mathrm{m})$, respectively. Robot 3 is expected to be at $(-1\,\mathrm{m}, 0.5\,\mathrm{m})$ in the local frame of Robot 2. Three features satisfying Assumption 1 are installed on each of Robots 1 and 2. A pan-controlled camera is equipped on each of Robots 2–4 with the offset $d = 0.1\,\mathrm{m}$. It should be noted that the value of the offset d is unknown to the robots. Three cameras are identical, and the intrinsic camera parameters are set as the calibration results of a Sony EVI-D70P PTZ-camera (see Table 2). The image size is 768×576 pixels. Random noise with the standard deviation of 0.5 pixel is added to the image.

For each of Robots 2–4, the formation controller (26) with the update laws (30)–(32) is used to realise the desired formation, and the camera controller (49) with the update laws (52)–(54) is used to track the visual features. The control-related parameters for Robots 2–4 are set equally. Table 3 shows the bounds of d, v_{l}, w_z, d_z, α and v_z. All parameters related to the update laws (30)–(32) and (52)–(54) are listed in Table 4. The control

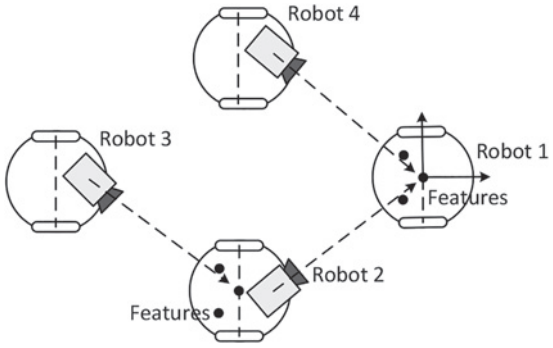

Fig. 3 *Diamond formation*

Table 2 Intrinsic camera parameters

f_y	f_z	m_0, pixel	n_0, pixel
902.1328	902.5014	420.7956	291.6529

Table 3 Bounds of unknown parameters

$\underline{c}_{\mathrm{d}}$	$\bar{c}_{\mathrm{d}}$	$\underline{c}_v$	$\bar{c}_v$	$\underline{\lambda}_w$	$\bar{\lambda}_w$	σ
0.04	0.16	0.01	0.7	−0.1	0.1	0.02
$\underline{\lambda}_{\mathrm{d}}$	$\bar{\lambda}_{\mathrm{d}}$	$\underline{\lambda}_\alpha$	$\bar{\lambda}_\alpha$	$\underline{\lambda}_v$	$\bar{\lambda}_v$	δ
0.2	1.8	2	10	0.1	7	0.25

Table 4 Parameters related to the update laws

γ_d	γ_v	γ_w	ε_d	ε_v	ε_w
0.01	0.03	0.003	0.01	0.01	0.01
μ_d	μ_α	μ_v	η_d	η_α	η_v
0.0001	0.0001	0.0001	0.1	0.1	0.1
$\hat{d}(0)$	$\hat{v}_l(0)$	$\hat{w}_z(0)$	$\hat{d}_z(0)$	$\hat{\alpha}(0)$	$\hat{v}_z(0)$
0.12	0.05	0	1	6	1

gains are set as $k_x = 0.1$, $k_y = 0.01$, $k_c = 0.5$ and the control circle is 50 ms. The initial poses for Robots 1–4 are (0 m, 0 m, $\frac{\pi}{2}$ rad), (1 m, −2 m, $\frac{\pi}{2}$ rad), (0 m, −5 m, $\frac{\pi}{2}$ rad) and (−1.5 m, −3 m, $\frac{\pi}{2}$ rad), respectively. Robot 1 travels along a circular curve with $v_l = 0.25$ m/s and $w_l = \frac{\pi}{60}$ rad/s. The calibration procedure to get the desired follower positions stated in Section 2.2 is implemented before formation control.

Figs. 4 and 5 show the simulation results. In Fig. 4*a*, the black rectangle indicates the camera and its orientation. It can be observed that all cameras orientate towards the corresponding leaders, and Robots 2–4 finally reach their desired positions. Fig. 4*b* shows that for Robots 2–4 all three features are kept in the FOV of the camera. Fig. 5*a* presents the formation error $l_e = \sqrt{x_e^2 + y_e^2}$ and the image error e_y. It is clear that all errors eventually converge to zero. In Fig. 5*b*, all estimates of the unknown parameters are limited in the given bounds (see Table 3). Fig. 5*c* shows the control inputs. As random noise is added to the image, the control inputs are not smooth, which can be alleviated by increasing the number of feature points.

4.2 Experimental results

Two Pioneer 3-DX differential-driving mobile robots are used as the leader and the follower, respectively. A board with three infrared LEDs, which are distributed according to Assumption 1, is mounted on the leader. A Sony EVI-D70P PTZ-camera is installed on the follower. The intrinsic camera parameters are shown in Table 2. An infrared filter is attached on the camera to ensure that only the infrared light can get through the filter. Therefore the LEDs are observed as white area against the black background in the image. The image coordinates of the LEDs are extracted by the thresholding algorithm. The follower is placed at about 0.8 m behind the leader to implement the calibration procedure stated in Section 2.2 to obtain the desired follower position. The initial pose of the follower is at the right-hand side behind the leader with the camera roughly pointing to the LEDs. The leader moves along a circle with $v_l = 0.15$ m/s and $w_l = 0.125$ rad/s. The control gains are $k_x = 0.1$, $k_y = 0.01$ and $k_c = 0.5$. The control circle is about 150 ms. All other parameters are the same as that in the simulation (see Tables 2–4).

Figs. 6 and 7 report the experimental results. Fig. 6*a* shows that the formation can be well maintained. The feature trajectories in the image plane are shown in Fig. 6*b*. Clearly, the three LEDs are always observed. In Fig. 7*a*, the formation error $l_e = \sqrt{x_e^2 + y_e^2}$ and the image error e_y are eventually bounded in small neighbourhoods of zero, which means the desired formation is achieved and the camera orientation is adjusted to keep the LEDs observed. Fig. 7*b* reports that all estimates of the unknown parameters are constrained in the given bounds (see Table 3). The control inputs are presented in Fig. 7*c*. The red lines show the execution of the velocity commands (blue lines). It takes about 3 s for the follower to respond the linear velocity command because the maximum linear velocity of the follower is limited to be 0.4 m/s for the safety purpose. Since the pan angle of the PTZ-camera can only change

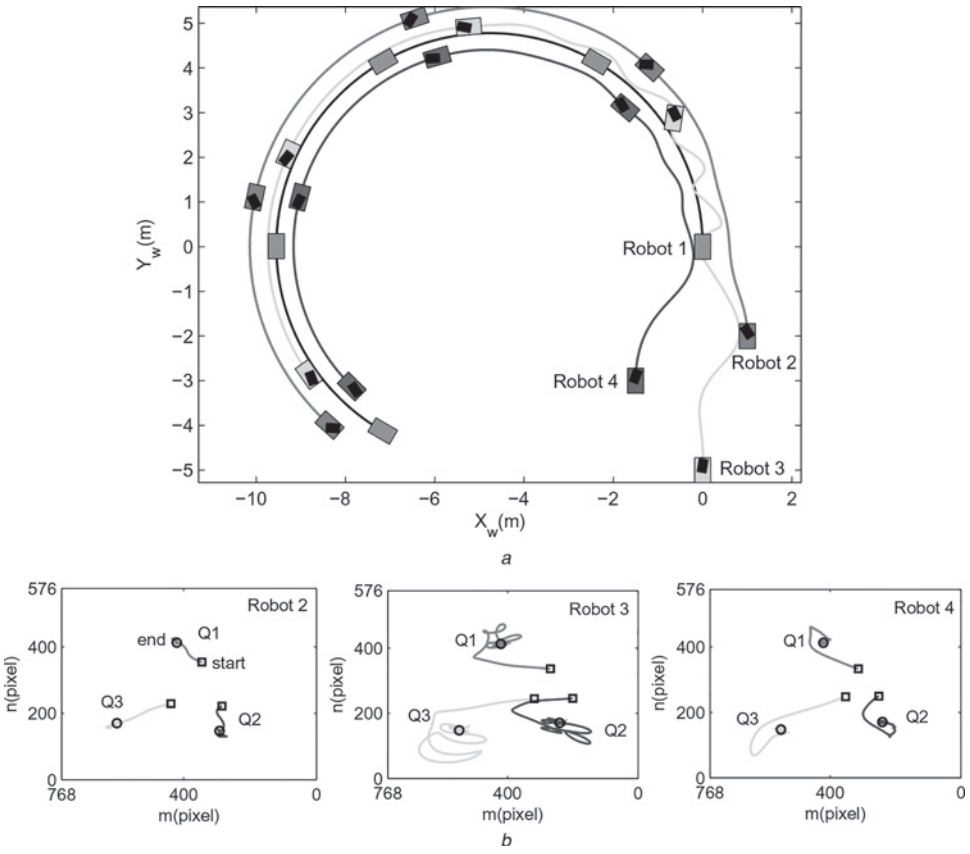

Fig. 4 *Simulation results*

a Robot trajectories
b Feature trajectories in the camera's image plane for Robots 2–4

IET Control Theory Appl., 2015, Vol. 9, Iss. 8, pp. 1302–1311

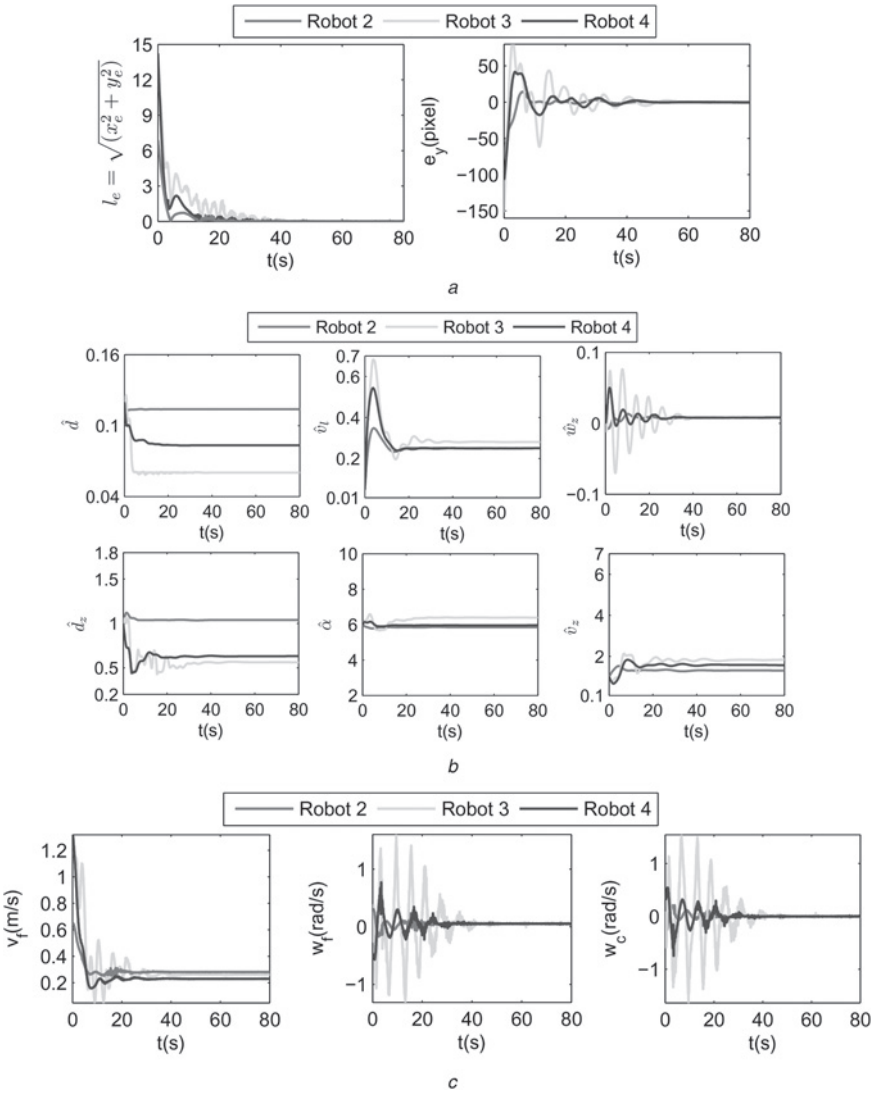

Fig. 5 *Simulation results*

a Formation error and image error
b Estimates of unknown parameters
c Control inputs

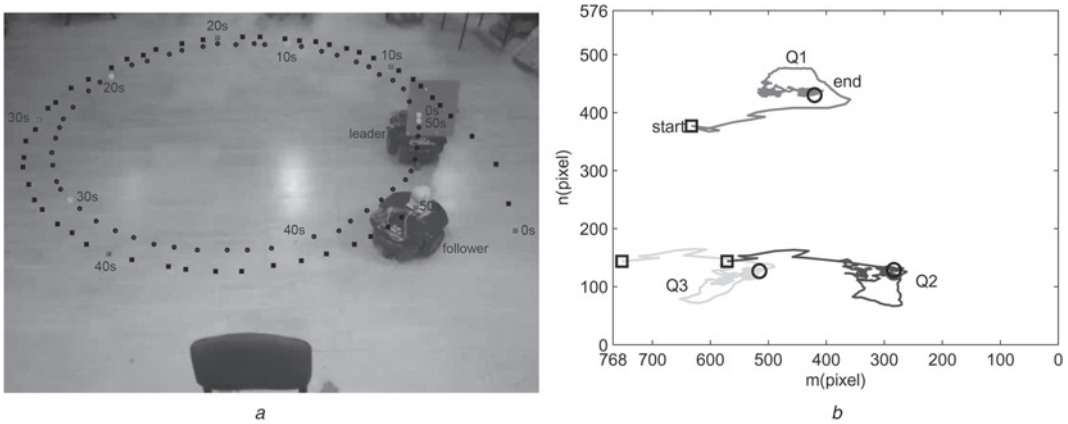

Fig. 6 *Experimental results*

a Robot trajectories captured by an overhead camera
b Feature trajectories in the camera's image plane

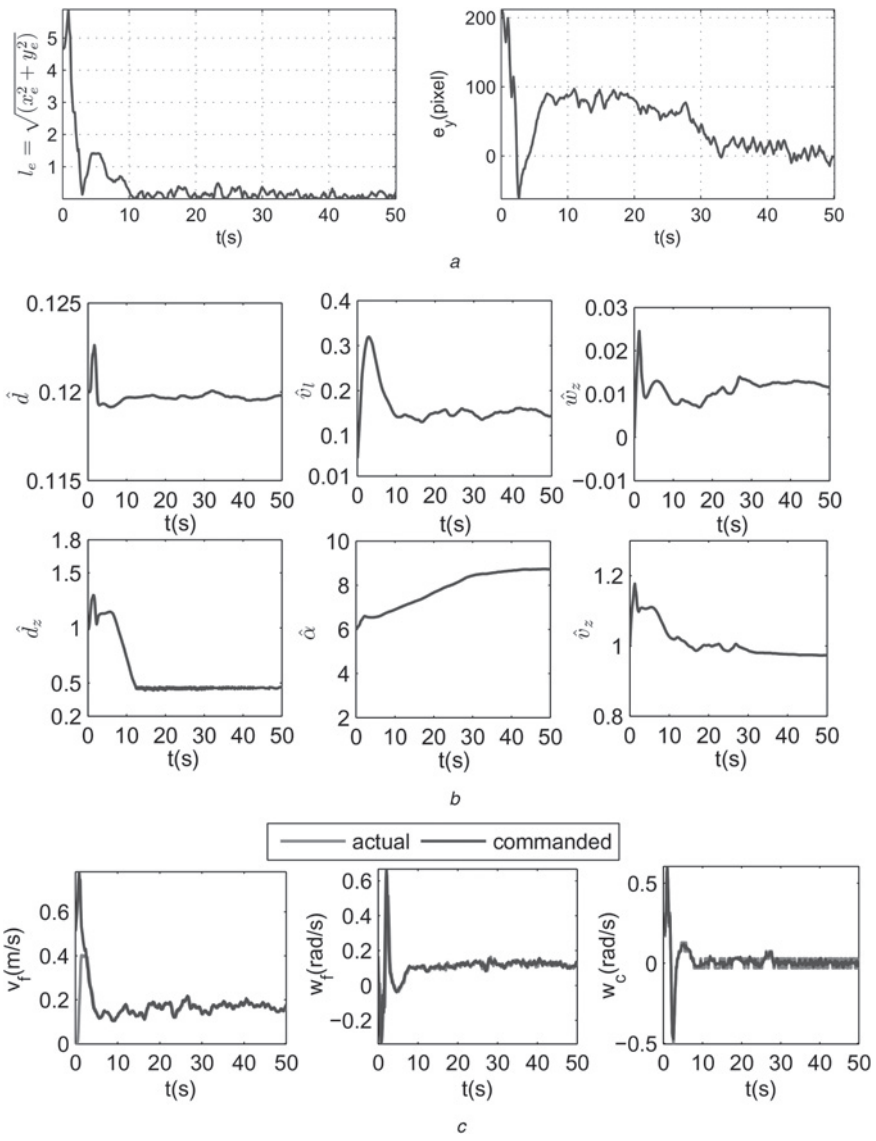

Fig. 7 *Experimental results*

a Formation error and image error
b Estimates of unknown parameters
c Control inputs

with 24 fixed speeds up to $\frac{\pi}{1.8}$ rad/s, the actual angular velocity of the camera is non-smooth.

5 Conclusions

This paper investigated the active vision-based leader-follower formation control of non-holonomic mobile robots in the absence of communication. A new vision-based formation system was proposed to eliminate the need of inter-robot range estimation. An adaptive formation controller and an adaptive camera controller were designed to achieve formation maintenance and target observation, respectively. The use of parameter projection algorithm bounded the control inputs, and consequently the input constraints of physical systems were alleviated. The effectiveness of our active vision-based formation control approach was verified by the simulation and experimental results.

6 Acknowledgment

The authors appreciate the helpful comments from the anonymous reviewers. This work was supported by the National Basic Research Program of China (973 Program: 2012CB821200, 2012CB821201), the NSFC (61134005, 61221061, 61327807), and the External-Planned Task (NO. SKLRS-2014-ZD-01) of the State Key Laboratory of Robotics and Systems (HIT).

7 References

1 Balch, T., Arkin, R.C.: 'Behavior-based formation control for multirobot team', *IEEE Trans. Robot. Autom.*, 1998, **14**, (6), pp. 926–939
2 Do, K.D., Pan, J.: 'Nonlinear formation control of unicycle-type mobile robots', *Robot. Auton. Syst.*, 2007, **55**, (3), pp. 191–204
3 Yoo, S.J., Park, J.B., Choi, Y.H.: 'Adaptive formation tracking control of electrically driven multiple mobile robots', *IET Control Theory Appl.*, 2010, **4**, (8), pp. 1489–1500
4 Ren, W., Sorensen, N.: 'Distributed coordination architecture for multi-robot formation control', *Robot. Auton. Syst.*, 2008, **56**, (4), pp. 324–333
5 Shao, J., Xie, G.M., Wang, L.: 'Leader-following formation control of multiple mobile vehicles', *IET Control Theory Appl.*, 2007, **1**, (2), pp. 545–552
6 Consolini, L., Morbidi, F., Prattichizzo, D., Tosques, M.: 'Leader-follower formation control of nonholonomic mobile robots with input constraints', *Automatica*, 2008, **44**, (5), pp. 1343–1349
7 Choi, K., Yoo, S.J., Park, J.B., Choi, Y.H.: 'Adaptive formation control in absence of leader's velocity information', *IET Control Theory Appl.*, 2010, **4**, (4), pp. 521–528

8 Sun, T., Liu, F., Pei, H., He, Y.: 'Observer-based adaptive leader-following formation control for non-holonomic mobile robots', *IET Control Theory Appl.*, 2012, **6**, (18), pp. 2835–2841
9 Peng, Z.X., Wen, G.G., Rahmani, A., Yu, Y.G.: 'Leader-follower formation control of nonholonomic mobile robots based on a bioinspired neurodynamic based approach', *Robot. Auton. Syst.*, 2013, **61**, (9), pp. 988–996
10 Moshtagh, N., Michael, N., Jadbabaie, A., Daniilidis, K.: 'Vision-based, distributed control laws for motion coordination of nonholonomic robots', *IEEE Trans. Robot.*, 2009, **25**, (4), pp. 851–860
11 Benhimane, S., Malis, E., Rives, P., Azinheira, J.R.: 'Vision-based control for car platooning using homography decomposition'. Proc. Int. Conf. Robotics and Automation, 2005, pp. 2161–2166
12 Vela, P., Betser, A., Malcolm, J., Tannenbaum, A.: 'Vision-based range regulation of a leader-follower formation', *IEEE Trans. Control Syst. Technol.*, 2009, **17**, (2), pp. 442–448
13 Cook, J., Hu, G.Q., Feng, Z.: 'Cooperative state estimation in vision-based robot formation control via a consensus method'. Proc. Chinese Control Conf., 2012, pp. 6461–6466
14 Das, A.K., Fierro, R., Kumar, V., Ostrowsky, J.P., Spletzer, J., Taylor, C.: 'A vision-based formation control framework', *IEEE Trans. Robot. Autom.*, 2002, **18**, (5), pp. 813–825
15 Vidal, R., Shakernia, O., Sastry, S.: 'Following the flock: distributed formation control with omnidirectional vision-based motion segmentation and visual servoing', *IEEE Robot. Autom. Mag.*, 2004, **11**, (4), pp. 14–20
16 Mariottini, G.L., Morbidi, F., Prattichizzo, D. *et al.*: 'Vision-based localization for leader-follower formation control', *IEEE Trans. Robot.*, 2009, **25**, (6), pp. 1431–1438
17 Morbidi, F., Mariottini, G.L., Prattichizzo, D.: 'Observer design via immersion and invariance for vision-based leader-follower formation control', *Automatica*, 2010, **46**, (1), pp. 148–154
18 Bakhtari, A., Benhabib, B.: 'An active vision system for multitarget surveillance in dynamic environments', *IEEE Trans. Syst., Man, Cybern., B, Cybern.*, 2007, **37**, (1), pp. 190–198
19 Fang, Y.C., Liu, X., Zhang, X.B.: 'Adaptive active visual servoing of nonholonomic mobile robots', *IEEE Trans. Ind. Electron.*, 2012, **59**, (1), pp. 486–497
20 Orqueda, O., Fierro, R.: 'Robust vision-based nonlinear formation control'. Proc. American Control Conf., 2006, pp. 1422–1427
21 Kannan, H., Chitrakaran, V.K., Dawson, D.M., Burg, T.: 'Vision-based leader/follower tracking for nonholonomic mobile robots'. Proc. American Control Conf., 2007, pp. 2159–2164
22 Fidan, B., Gazi, V., Zhai, S., Cen, N., Karatas, E.: 'Single-view distance-estimation-based formation control of robotic swarms', *IEEE Trans. Ind. Electron.*, 2013, **60**, (12), pp. 5781–5791
23 Huang, J.S., Wen, C.Y., Wang, W., Jiang, Z.P.: 'Adaptive stabilization and tracking control of a nonholonomic mobile robot with input saturation and disturbance', *Syst. Control Lett.*, 2013, **62**, (3), pp. 234–241
24 Chen, X.H., Jia, Y.M.: 'Input-constrained formation control of differential-drive mobile robots: geometric analysis and optimization', *IET Control Theory Appl.*, 2014, **8**, (7), pp. 522–533
25 Zhang, Z.: 'A flexible new technique for camera calibration', *IEEE Trans. Pattern Anal. Mach. Intell.*, 2000, **22**, (11), pp. 1330–1334
26 Zhang, X.B., Fang, Y.C.: 'Motion-estimation-based visual servoing of nonholonomic mobile robots', *IEEE Trans. Robot.*, 2011, **27**, (6), pp. 1167–1175
27 Khalil, H.K.: 'Nonlinear systems' (Prentice-Hall, 2002, 3rd edn.)